Supplementary Materials

Oceanic repeaters boost the global climatic impact of the Tibetan Plateau

Yongkun Xie[a], Jianping Huang[a]*, Guoxiong Wu[b,c]*, Yimin Liu[b,c], Wenhao Dong[d,e], Mengmeng Lu[f,g], Bian He[b,c], Zifan Su[a,h], Qing Bao[b,c], Qingyun Zhao[a], Yuzhi Liu[a]

Contents:

[a] Collaborative Innovation Center for Western Ecological Safety, Lanzhou University, Lanzhou, China
[b] State Key Laboratory of Numerical Modeling for Atmospheric Sciences and Geophysical Fluid Dynamics (LASG), Institute of Atmospheric Physics, Chinese Academy of Sciences, Beijing, China
[c] College of Earth and Planetary Sciences, University of Chinese Academy of Sciences, Beijing, China
[d] NOAA/Geophysical Fluid Dynamics Laboratory, Princeton, NJ, USA
[e] Cooperative Programs for the Advancement of Earth System Science, University Corporation for Atmospheric Research, Boulder, CO, USA
[f] State Key Laboratory of Severe Weather and Institute of Climate System, Chinese Academy of Meteorological Sciences, Beijing, China
[g] Southern Marine Science and Engineering Guangdong Laboratory (Zhuhai), Zhuhai, China
[h] College of Atmospheric Sciences, Lanzhou University, Lanzhou, China.
* Corresponding author: Jianping Huang, hjp@lzu.edu.cn; Guoxiong Wu, gxwu@lasg.iap.ac.cn

Supplementary Data and methods

1. GPCP

The Global Precipitation Climatology Project (GPCP), version 2.3, dataset has a resolution of 2.5° × 2.5° and is available for the period ranging from January 1979 to the present. The GPCP is provided by NOAA/OAR/ESRL PSL, Boulder, Colorado, USA and can be accessed from https://psl.noaa.gov/data/gridded/data.gpcp.html.

2. GISTEMP

The Goddard Institute for Space Studies (GISS) Surface Temperature Analysis (GISTEMP), version 4, dataset has a resolution of 2° × 2° and is available for the period ranging from January 1880 to the present. The GISTEMP is provided by NASA/GISS and can be accessed from https://data.giss.nasa.gov/gistemp/.

3. ERA5

The fifth-generation ECMWF reanalysis dataset (ERA5) is the latest version of the ECMWF reanalysis and is available for the period ranging from January 1950 to the present, wherein single-level surface data were used. ERA5 data are in monthly mean and have a resolution of 1° × 1°. The variables examined were 2 m air temperature. ERA5 data can be accessed at the ECMWF website https://www.ecmwf.int/en/forecasts/datasets/reanalysis-datasets/era5.

4. NCEP-2

NCEP-DOE Reanalysis-2 (NCEP-2) monthly sigma-level fields of diabatic heating of the atmosphere provide six separate components of diabatic heating, which allowed us to examine the individual physical processes contributing to total diabatic heating. The six physical process-based components were solar and longwave radiative, vertical diffusion (sensible heat), large-scale condensation, and deep and shallow convective heat. NCEP-2 is in a global T62 Gaussian grid with 28 vertical sigma levels, available for the period ranging from January 1979 to August 2014. NCEP-2 data can be accessed at http://iridl.ldeo.columbia.edu/SOURCES/.NOAA/.NCEP-DOE/.Reanalysis-2/.Monthly/.dg3/.dg3/.

5. Numerical simulations

GMMIP officially proposed six experiments, two of which were useful for our study—amip-hist and amip-TIP-nosh (Table S1). Among all the models that participated in GMMIP, only two, i.e., FGOALS-f3-L and FIO-ESM-2-0, had all the outputs of the three required experiments available. GMMIP data are available to the public on the CMIP6 website: https://esgf-node.llnl.gov/search/cmip6/.

6. Statistical significance of the difference and correlation

To determine the statistical significance (95% confidence level) of the difference between the control and sensitivity runs, a two-tailed Student's *t*-test was performed. The function of the *t*-test is documented on the NCL website https://www.ncl.ucar.edu/Document/Functions/Built-in/ttest.shtml. The statistical significance (95% confidence level) of the correlation coefficient was determined using a two-tailed Pearson's *r*-test. The function used to calculate the correlation coefficient is documented at https://www.ncl.ucar.edu/Document/Functions/Built-in/escorc.shtml, while the function of the *r*-test is documented at https://www.ncl.ucar.edu/Document/Functions/Built-in/rtest.shtml.

Supplementary Figures S1–S14

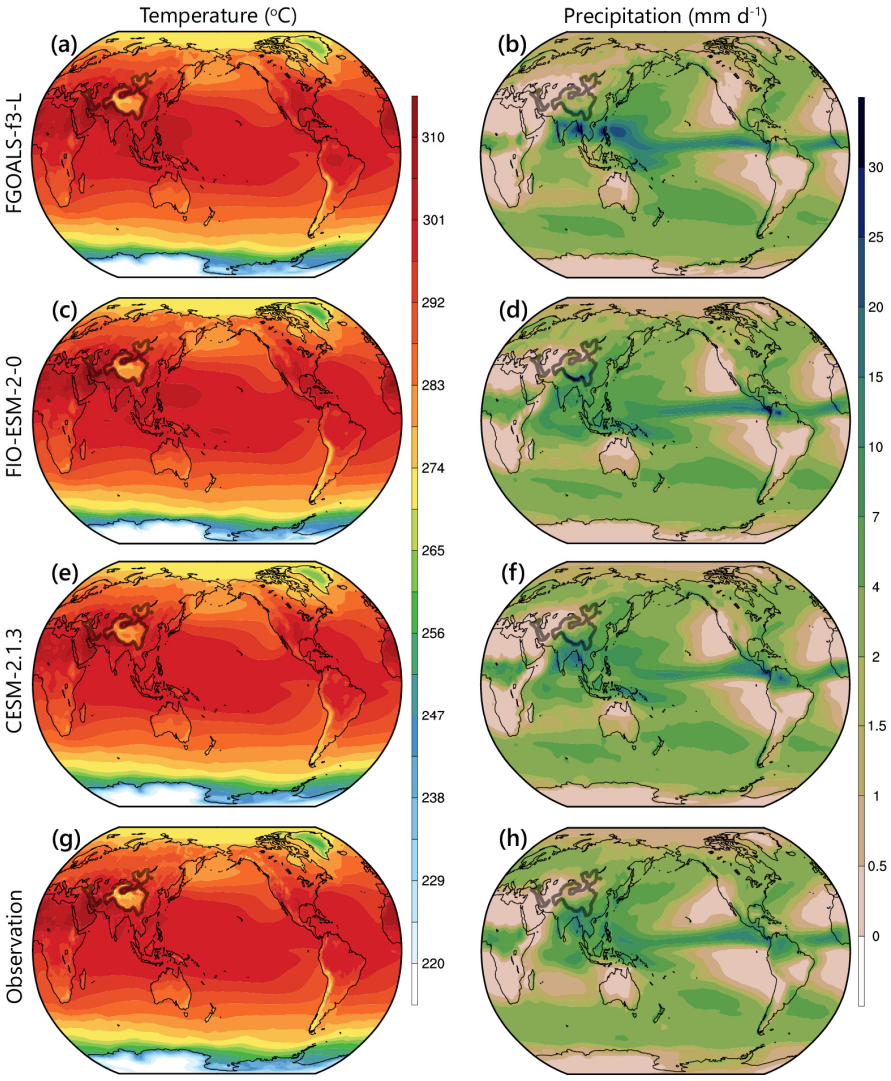

Fig. S1. Climatology of the June to August (JJA) mean temperature and precipitation. Near-surface air temperature and precipitation averaged from 1979–2014 based on amip-hist experiment of (a, b) FGOALS-f3-L, (c, d) FIO-ESM-2-0, and (e, f) CESM-2.1.3 models and from observational data of (g) ERA5 and (h) GPCP. The thick grey contour indicates 1.5 km elevation.

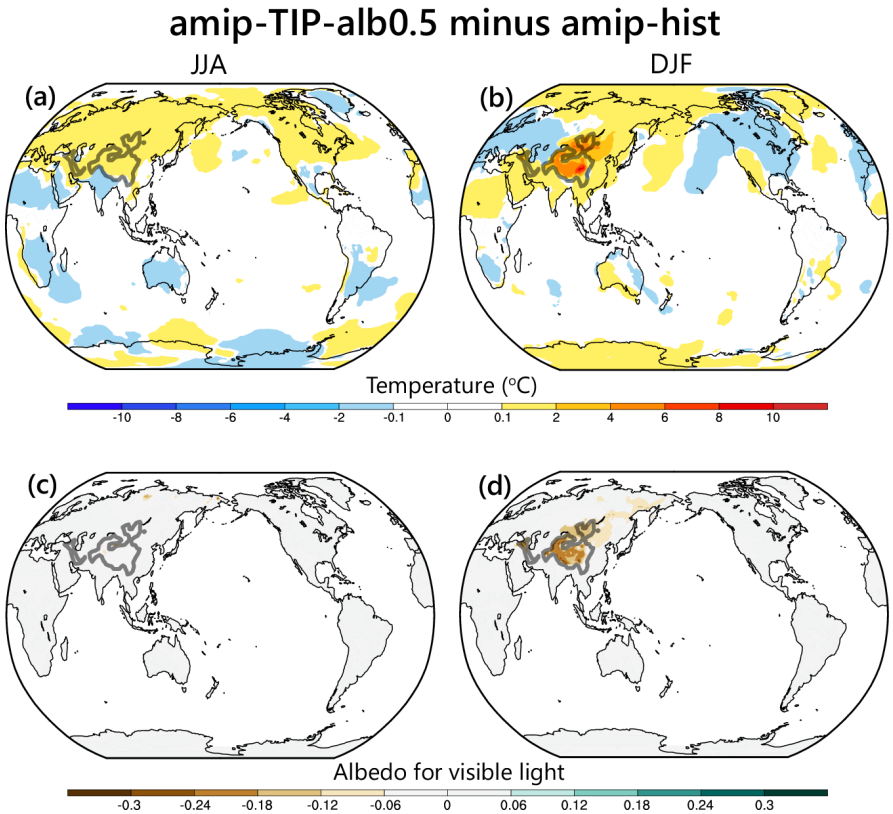

Fig. S2. Spatial pattern of anomalous TP heating in the half-albedo experiment. Differences in JJA and DJF mean (a, b) near-surface air temperature and (c, d) albedo for visible light determined using amip-TIP-alb0.5 minus amip-hist for 1979–2014. The thick grey contour indicates 1.5 km elevation.

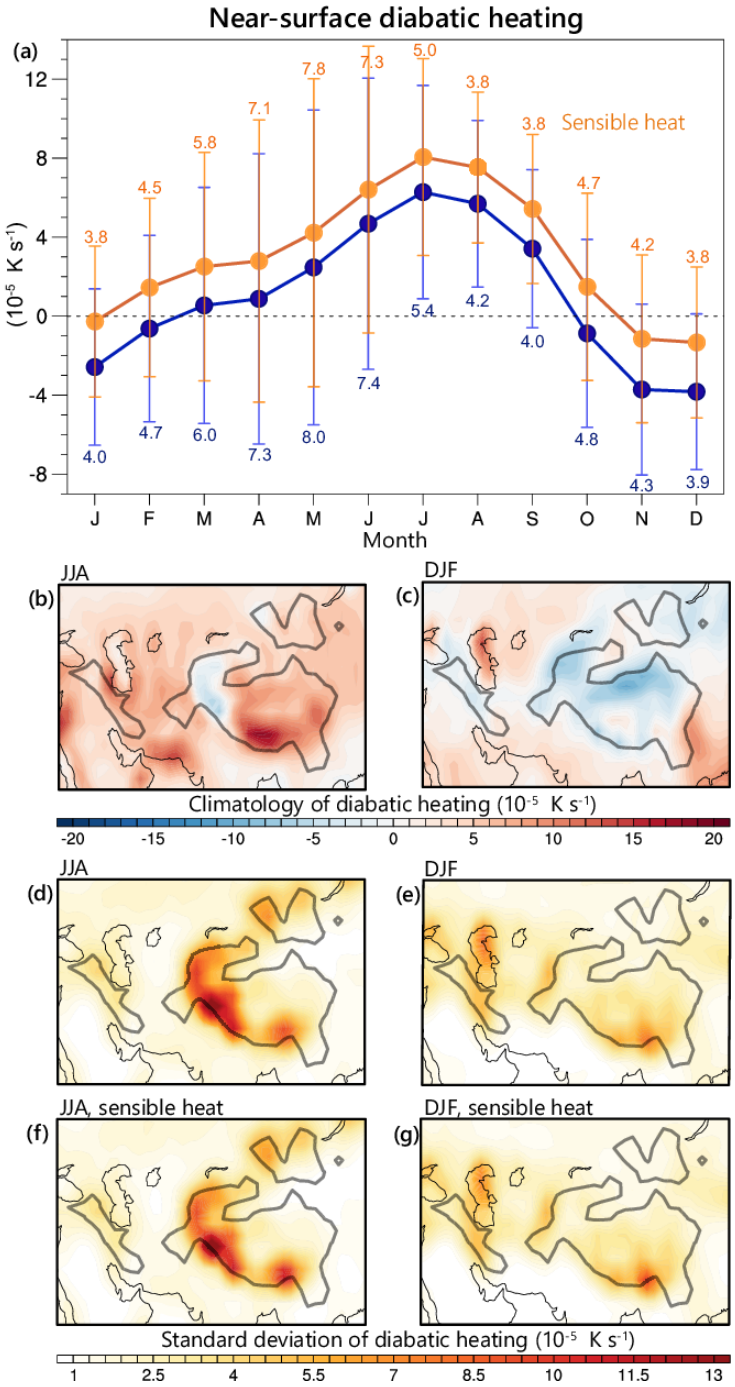

Fig. S3. Seasonality and patterns of TP heating. (a) Monthly mean diabatic heating at 0.995 sigma level (blue) and its component contributed by sensible heat (orange), averaged over the TP domain higher than 1.5 km from NCEP-2 data, for 1979–2014. The vertical bar indicates the range of one standard deviation (number). (b), (c) Spatial patterns of the climatological diabatic heating in JJA and DJF. (d), (e) Spatial patterns of the standard deviation of diabatic heating in JJA and DJF. (f, g) Same as (d, e) but for the sensible heat component. The thick grey contour indicates 1.5 km elevation.

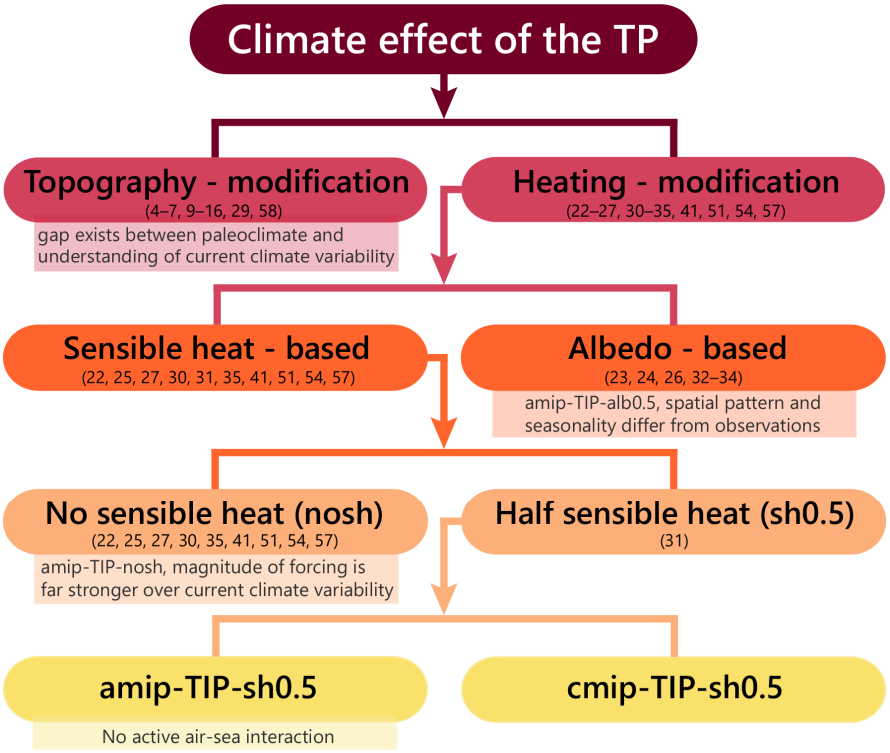

Fig. S4. Schematic summary of the categories of experimental designs used for simulating the climate effect of the TP. Limitations of the experiments in terms of our research purpose are noted in the drop-down panel. The previous studies that have used each experimental design are also marked.

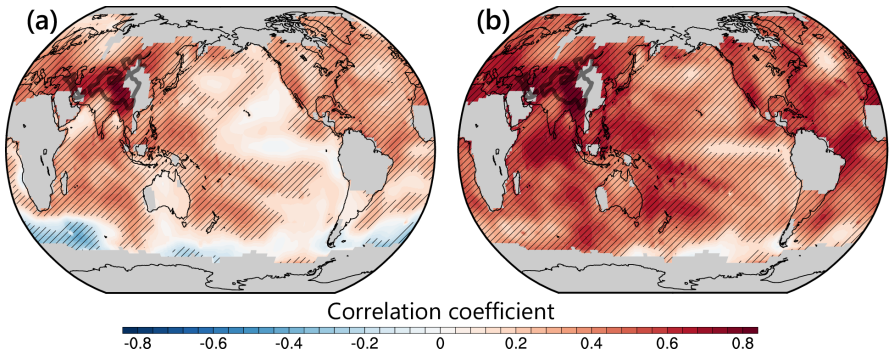

Fig. S5. The correlation of the TP temperature with the global temperature. (a) The correlation coefficient between the JJA mean near-surface air temperature averaged over the TP domain higher than 1.5 km with global near-surface air temperature after linear detrending for 1880–2022, based on GISTEMP data. (b) Same as (a) but for result without linear detrending. The stripe indicates significant correlation at the 95% confidence level. The grey filling indicates the missing value in GISTEMP data. The thick grey contour indicates 1.5 km elevation.

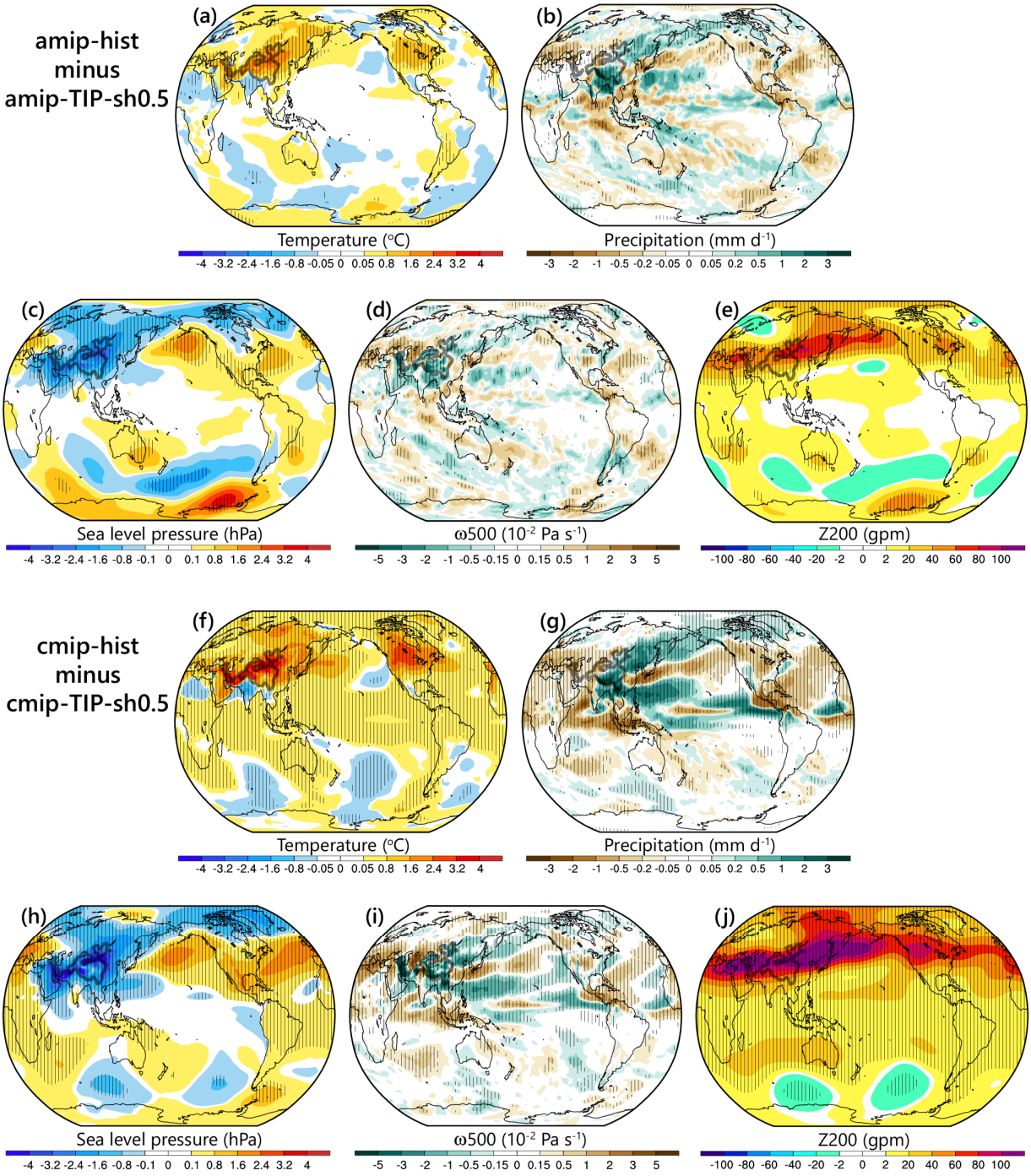

Fig. S6. Impact of TP heating on global climate in summer in amip and cmip experiments. Differences in JJA mean (a) near-surface air temperature, (b) precipitation, (c) sea level pressure, (d) ω500, and (e) Z200 determined using amip-hist minus amip-TIP-sh0.5 for 1979–2014. (f–j) Same as (a–e) but for cmip-hist minus cmip-TIP-sh0.5 for 1850–2014. The stripe indicates significant differences at the 95% confidence level. The thick grey contour indicates 1.5 km elevation.

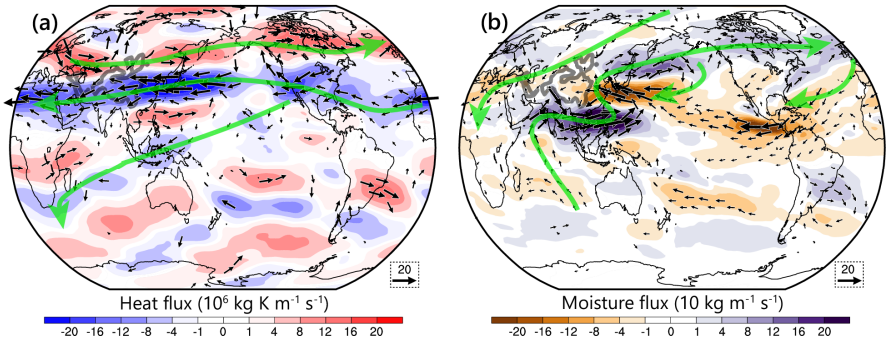

Fig. S7. Impact of air-sea interactions on horizontal heat and moisture transport. Differences in JJA mean vertically-integrated horizontal (a) heat and (b) moisture flux (vector) and their zonal components (color shading) determined using cmip (cmip-hist minus cmip-TIP-sh0.5) minus amip (amip-hist minus amip-TIP-sh0.5) experiments for 2000–2014. The vectors with insignificant (95% confidence level) differences in both zonal and meridional components were not shown; the green arrows indicate the pathways of heat or moisture flux. The thick grey contour indicates 1.5 km elevation.

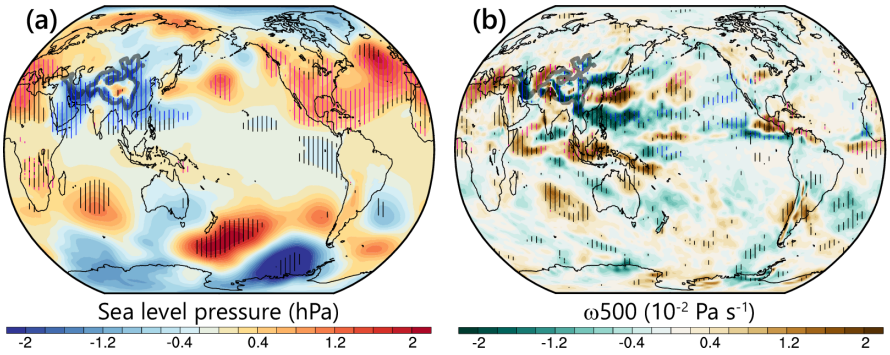

Fig. S8. Effect of air-sea interactions on sea level pressure and vertical motion. Differences in JJA mean (a) sea level pressure and (b) ω500 determined using cmip (cmip-hist minus cmip-TIP-sh0.5) minus amip (amip-hist minus amip-TIP-sh0.5) experiments for 1850–2014. The stripe indicates significant differences in cmip minus amip at the 95% confidence level; the red and blue colors further indicate all-positive and all-negative configurations in the signs of cmip, amip, and cmip minus amip. The thick grey contour indicates 1.5 km elevation.

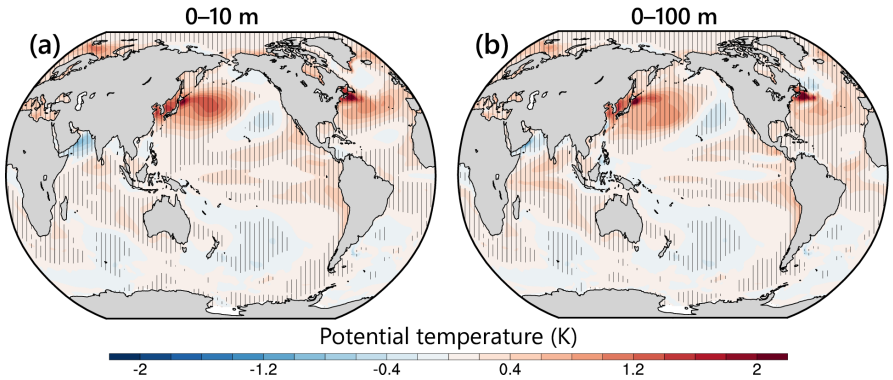

Fig. S9. Impact of TP heating on subsurface ocean temperature in summer. Differences in JJA mean subsurface ocean potential temperature for (a) 0–10 m and (b) 0–100 m layers determined using cmip-hist minus cmip-TIP-sh0.5 for 1850–2014. The stripe indicates significant differences at the 95% confidence level.

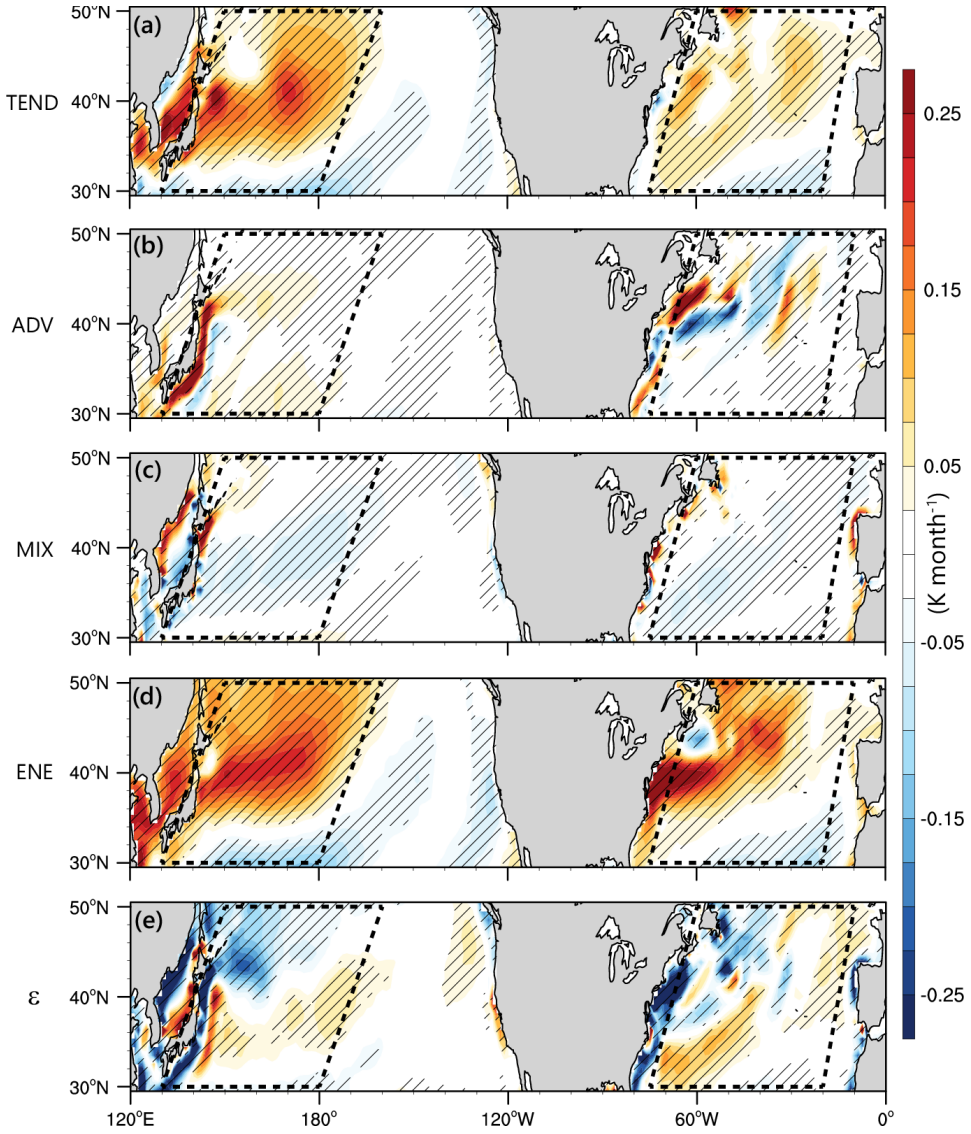

Fig. S10. Impact of TP heating on the energy budget of the ocean mixed layer over the North Pacific and Atlantic domains. Differences in JJA mean energy budget terms of the mixed layer as indicated in Eq. (1), as determined using cmip-hist minus cmip-TIP-sh0.5 experiments for 1850–2014. The stripe indicates significant differences at the 95% confidence level.

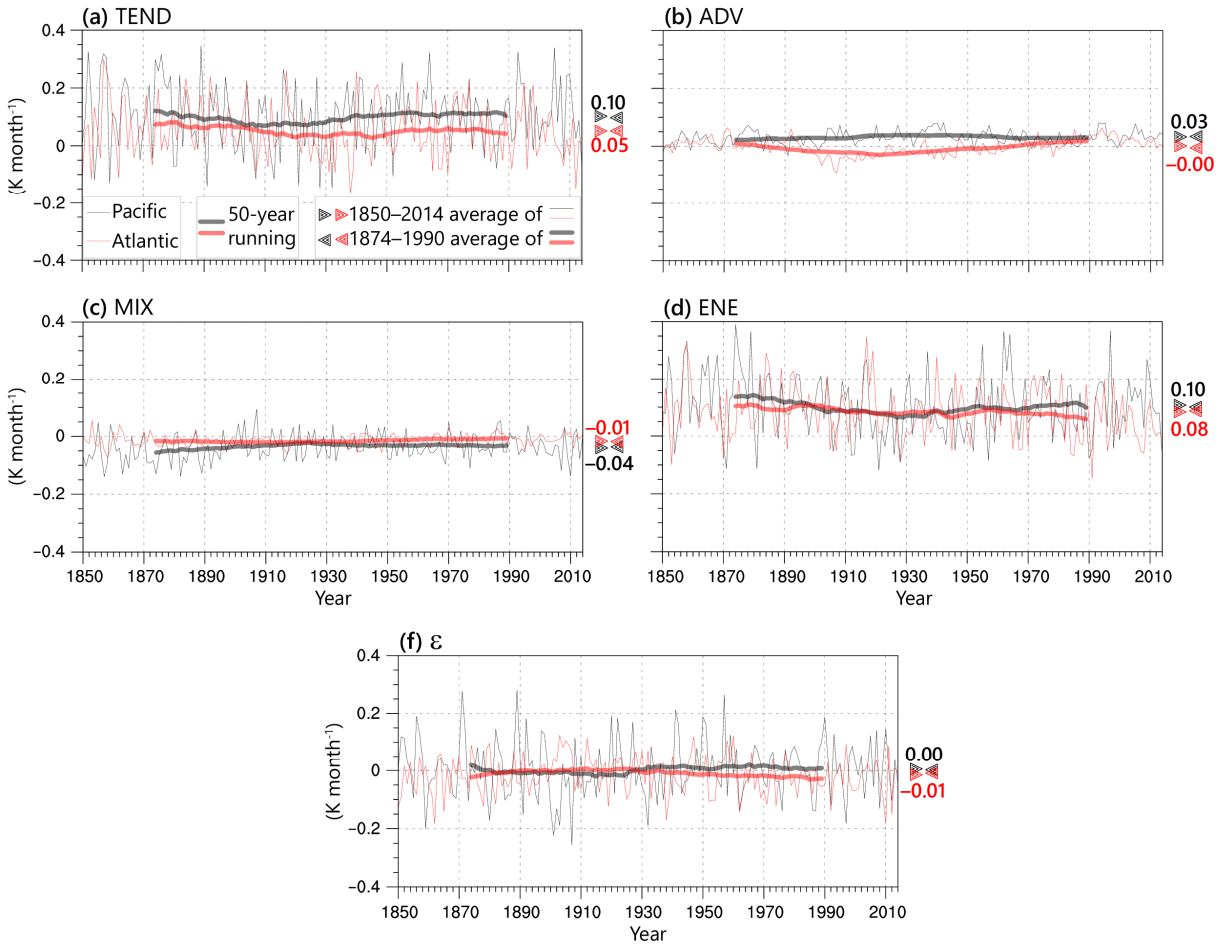

Fig. S11. Time-series of the differences in JJA mean energy budget terms (Eq. (1)) of mixed layer averaged over the Pacific (black) and Atlantic (red) domains shown in Fig. 3a, determined using cmip-hist minus cmip-TIP-sh0.5 experiments. The thin lines indicate the raw time-series for 1850–2014, while the thick lines indicate the 50-year-running-mean time-series for 1874–1990. The triangle markers indicate the temporal averages of the raw and 50-year-running-mean time-series, and the numbers indicate their average values. Fig. 4a also shows the averaged results for 1850–2014.

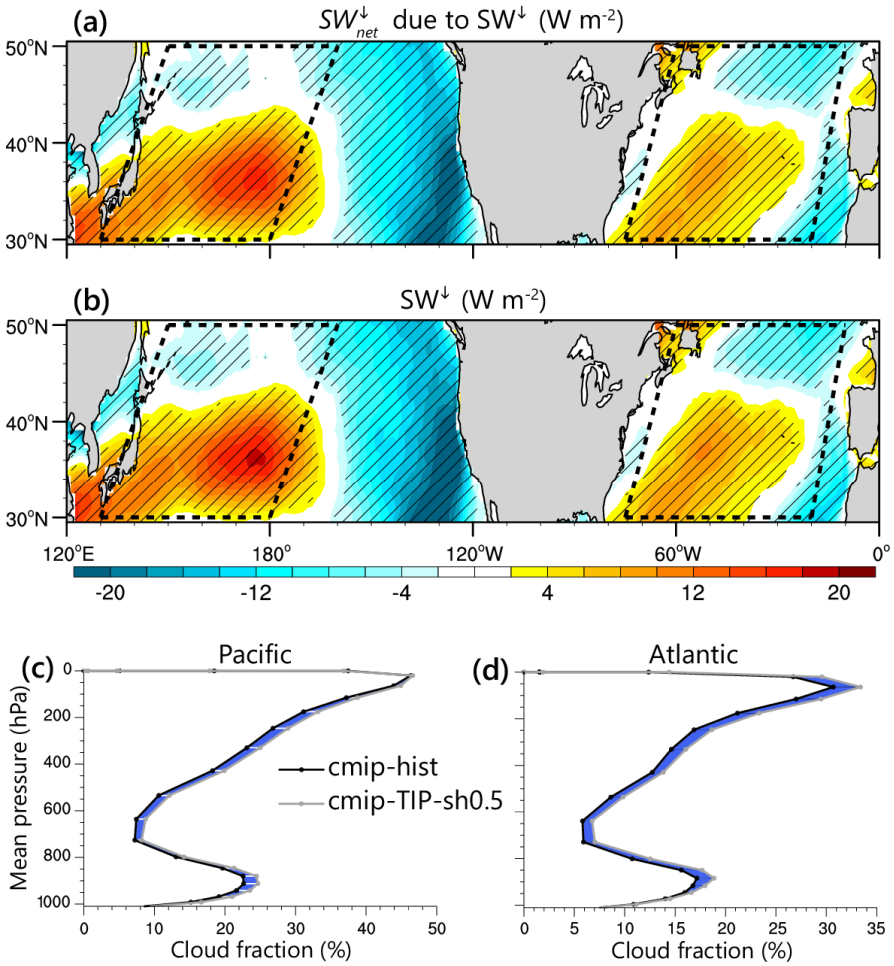

Fig. S12. Physical processes underlying the changes in net shortwave at the sea surface over the Pacific and Atlantic domains in summer. Differences in JJA mean (a) net shortwave ($SW^{\downarrow}_{net}$) due to downward shortwave ($SW^{\downarrow}$) formulated as the last right-hand term of $\delta(SW^{\downarrow}_{net}) \approx \underbrace{\delta(1-\alpha)SW^{\downarrow}}_{\text{Albedo feedback}} + \underbrace{(1-\alpha)\delta(SW^{\downarrow})}_{SW^{\downarrow}\text{ change}}$, (b) downward shortwave determined using cmip-hist minus cmip-TIP-sh0.5 experiments for 1850–2014. (c), (d) Regional mean cloud fraction averaged over the Pacific and Atlantic domains with positive value in (a) for cmip-hist and cmip-TIP-sh0.5 experiments, respectively. The blue shadings indicate that differences using the cmip-hist minus cmip-TIP-sh0.5 are negative, namely a reduced cloud fraction. The stripe indicates significant differences at the 95% confidence level.

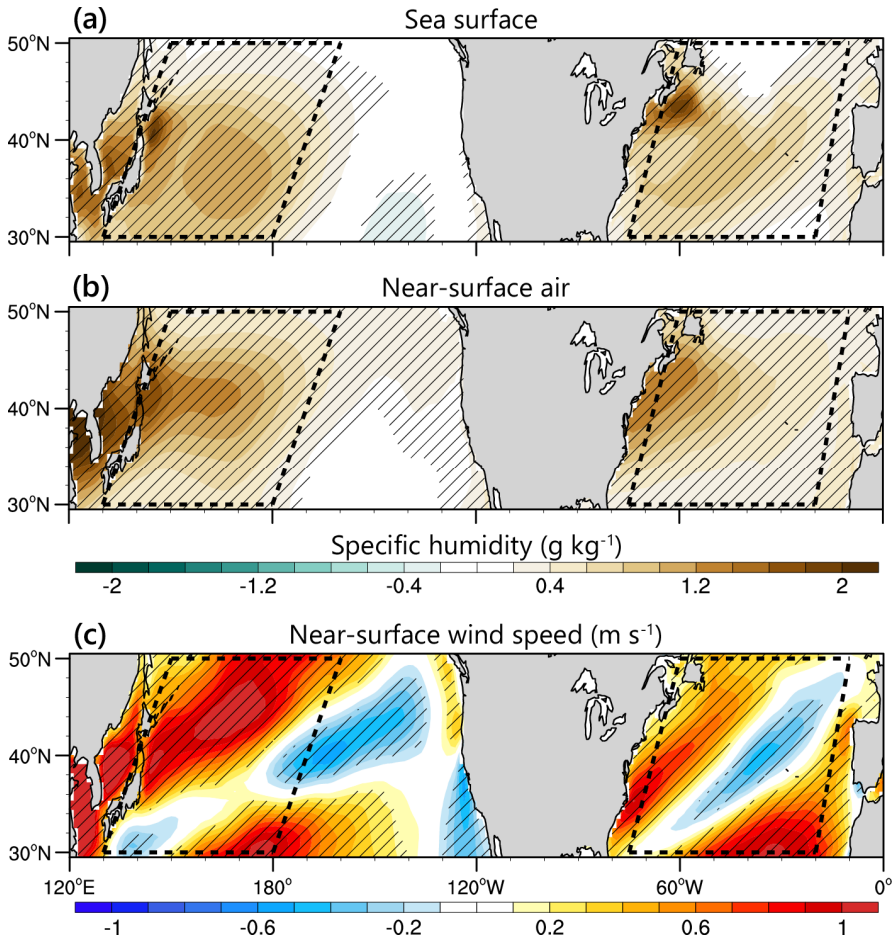

Fig. S13. Impact of TP heating on specific humidity and wind speed over the Pacific and Atlantic domains in summer. Differences in JJA mean (a) saturation specific humidity at sea surface temperature and (b) specific humidity of near-surface air determined using cmip-hist minus cmip-TIP-sh0.5 experiments for 1850–2014. The stripe indicates significant differences at the 95% confidence level. (c) Same as (b) but for near-surface wind speed.

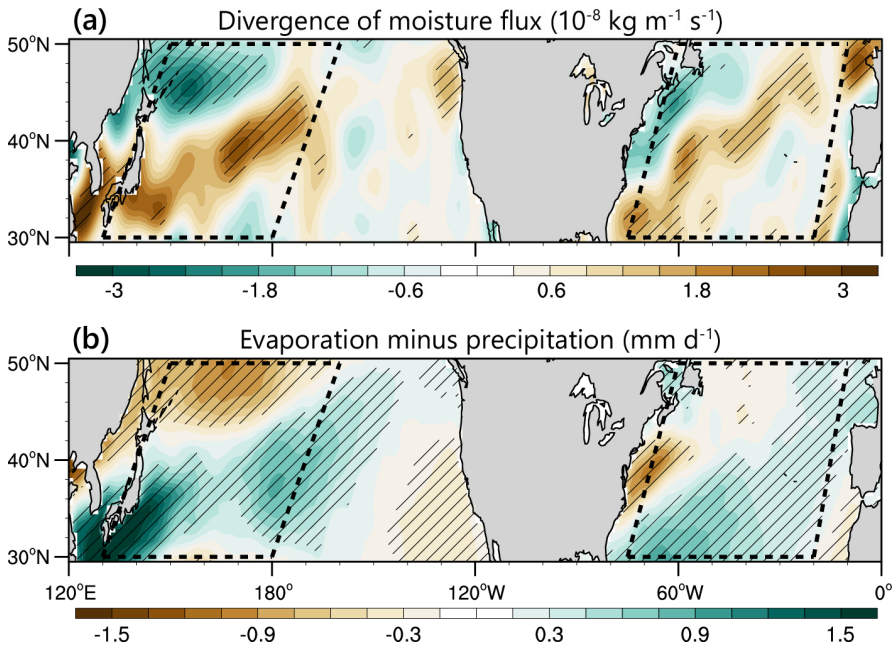

Fig. S14. Impact of TP heating on atmospheric specific humidity over the Pacific and Atlantic domains in summer. (a) Differences in JJA mean divergence of moisture flux, that is $\nabla_h \cdot \vec{M}$ ($\vec{M} = \rho \vec{V} q$; Section 2.3), at the near-surface, determined using cmip-hist minus cmip-TIP-sh0.5 experiments for 2000–2014. A negative value indicates convergence of atmospheric moisture. The stripe indicates significant differences at the 95% confidence level. (b) Same as (a) but for evaporation minus precipitation at the sea surface. A positive value indicates an increase in moisture source to the atmosphere from the sea surface. Since negative and positive values in (a) and (b) indicate positive contributions to atmospheric specific humidity, respectively, the color bars were opposite in (a) and (b).

Supplementary Table S1

Table S1. Information of models and experimental designs.

Models			
Name	Resolution		Institute
FGOALS-f3-L	Atmos: FAMIL2.2, c96 finite volume grid; 180 × 360 lat/lon; 32 vertical levels		IAP-LASG/China
FIO-ESM-2-0	Atmos: CAM4, 0.9 × 1.25 finite volume grid; 192 × 288 lat/lon; 26 vertical levels		FIO/China
CESM-2.1.3	Official tag: f09_f09_mg17 for amip and f09_g17 for cmip Atmos: CAM6, 0.9 × 1.25 finite volume grid; 192 × 288 lat/lon; 32 vertical levels Land: CLM5.0, 0.9 × 1.25 finite volume grid Ocean: POP2, finite volume grid 0.9 × 1.25_g × 1v7		NCAR/UCAR/USA
GMMIP experiments			
Name*	Designs	Time	Models
amip-hist	The historical run commences from January 1, 1861, with the external forcing defined by the observed values.	1861–2014	FGOALS-f3-L FIO-ESM-2-0
amip-TIP-nosh	Sensible heat is removed over the Asian topographies above 500 m [35]. The method used by FGOALS-f3-L is to set the vertical temperature diffusion term to zero in the atmospheric thermodynamic equation at the bottom boundary layer.	1970–2014	
CESM experiments			
amip-hist amip-TIP-nosh	Modified from the official case: FHIST amip-hist: same as GMMIP experiments except for integration time. amip-TIP-nosh: modified from amip-hist by removing the vertical diffusive sensible	1979–2014	

	heat on the entire column of the atmosphere, that is, all the model levels over the Asian topographies (same domain as in GMMIP).	(three-hourly outputs for 2000–2014)	CESM-2.1.3
amip-TIP-alb0.5	Same as amip-TIP-nosh, except for modification in surface albedo. The albedo is multiplied by 0.5; hence, TP heating increases relative to amip-hist.		
amip-TIP-sh0.5	Modified from amip-TIP-nosh by multiplying the sensible heat by 0.5, instead of setting a zero sensible heat.		
cmip-hist	Modified from the official case: BHIST Same as amip-hist but for a run with all components fully active and a different integration time.	1850–2014 (three-hourly outputs for 2000–2014)	
cmip-TIP-sh0.5	Modified from cmip-hist. The code modification is the same as in amip-TIP-sh0.5.		

* Experiment names follow the rules of the GMMIP.